Twinning Superlattice Formation in GaAs Nanowires

Tim Burgess,[†,*] Steffen Breuer,[†] Philippe Caroff,[†] Jennifer Wong-Leung,[†,‡] Qiang Gao,[†] Hark Hoe Tan,[†] and Chennupati Jagadish[†,*]

[†]Department of Electronic Materials Engineering, Research School of Physics and Engineering and [‡]Centre for Advanced Microscopy, The Australian National University, Canberra, ACT 0200, Australia

ABSTRACT Semiconductor nanowires have proven a versatile platform for the realization of novel structures unachievable by traditional planar epitaxy techniques. Among these, the periodic arrangement of twin planes to form twinning superlattice structures has generated particular interest. Here we demonstrate twinning superlattice formation in GaAs nanowires and investigate the diameter dependence of both morphology and twin plane spacing. An approximately linear relationship is found between plane spacing and nanowire diameter, which contrasts with previous results reported for both InP and GaP. Through modeling, we relate this to both the higher twin plane surface energy of GaAs coupled with the lower supersaturation relevant to Au seeded GaAs nanowire growth. Understanding and modeling the mechanism of twinning superlattice formation in III–V nanowires not only provides fundamental insight into the growth process, but also opens the door to the possibility of tailoring twin spacing for various electronic and mechanical applications.

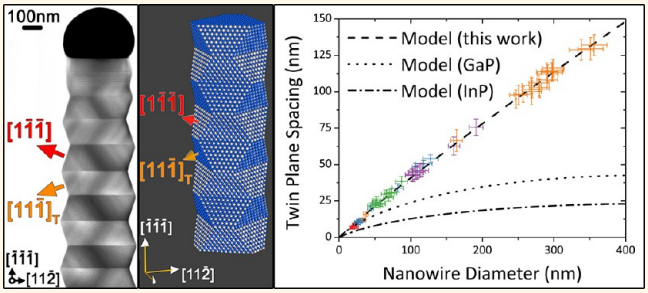

KEYWORDS: nanowire · III–V semiconductors · crystal structure · superlattice · twin planes · zincblende · gallium arsenide

As a nanoscale framework offering a tunable direct bandgap and high electron mobility, III–V compound semiconductor nanowires are the subject of significant research interest for both device application and fundamental physical study. Most commonly grown by the vapor–liquid–solid (VLS) mechanism, the successful demonstration of nanowire-based structures such as photovoltaic cells,[1–4] photodetectors,[5,6] lasers,[7] tunnel diodes,[8,9] and transistors,[10,11] has benefited from ongoing efforts to optimize material quality with a particular emphasis on planar defects and the related concept of crystal phase control.[12,13] Representing considerable novelty, periodic arrangements of twin planes termed twinning superlattices (TSL) have now been reported for a variety of III–V NW systems including InAs,[14–18] InP,[19–21] GaP,[22] and horizontally growing GaAs[23] with similar reports for other semiconductor materials including Zn_3P_2,[17,24] ZnTe,[25] ZnSe,[26–28] ZnS,[29] $ZnSnO_4$,[30] ZnO,[31] and SiC.[32] Beyond potential for fundamental insight into the growth process,[22] periodic twinning has been predicted to introduce electronic miniband structure, which may be useful for bandgap engineering, as well as direct intersubband optical transitions.[33–38] A reduction in thermal conductivity, which has been both modeled[39–41] and demonstrated,[42] holds further interest for thermoelectric application, while increased mechanical strength has been reported for twinned metallic nanowires[43,44]

Periodic twin plane formation in III–V nanowires has been widely reported to be promoted by zinc doping.[3,19,20,22,23,45] In their pioneering work on twinning superlattice formation in InP nanowires, Algra *et al.*[19] discussed several possible actions of this impurity. Taking both the results of modeling and the observation that zinc addition did not affect nanowire diameter, the authors suggested the most significant role of zinc was in reordering the Au-nanowire interface. Working again with InP nanowires, Wallentin *et al.*[46] have contrastingly reported a systematic increase in contact angle with increased zinc flow, explaining the discrepancy between works with reference to differing reactor cooling rates. Assuming a constant

* Address correspondence to tim.burgess@anu.edu.au; cxj109@physics.anu.edu.au.

Received for review July 3, 2013 and accepted August 29, 2013.

Published online August 29, 2013
10.1021/nn403390t

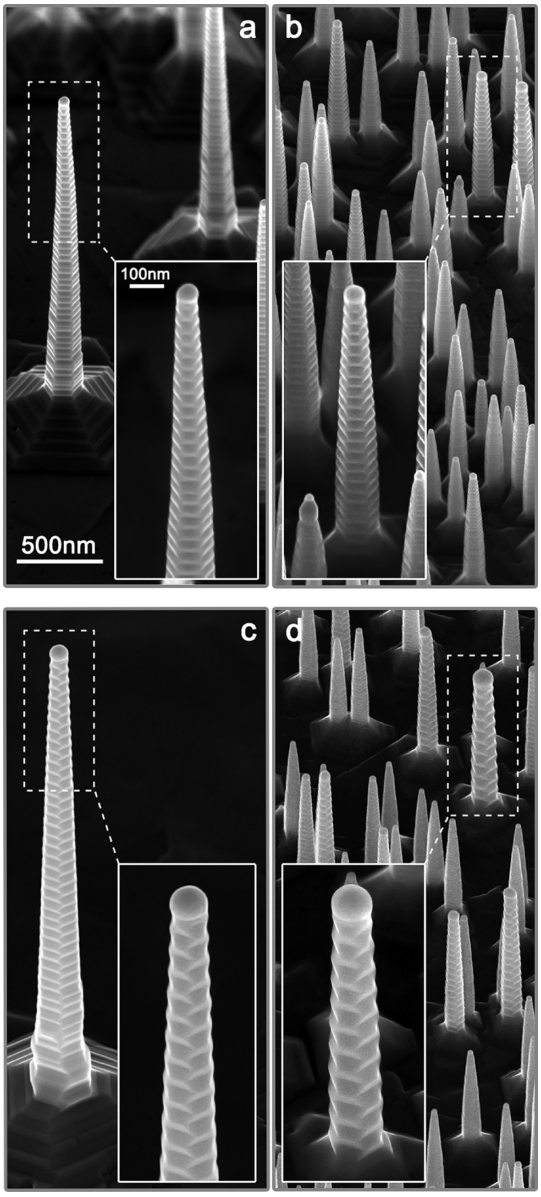

Figure 1. General nanowire morphology showing variation with both nanowire diameter and density: Each SEM image and corresponding inset show the same magnification where the sample substrate is tilted 45° relative to the incident electron beam; (a) Areal density of 0.21 nanowires/μm^2, where inset magnifies an approximately 50 nm diameter nanowire; (b) Areal density of 7.2 nanowires/μm^2, where inset magnifies an approximately 50 nm diameter nanowire; (c) Areal density of 0.09 nanowires/μm^2, where inset magnifies an approximately 100 nm diameter nanowire; (d) Areal density of 7.2 nanowires/μm^2, where inset magnifies an approximately 100 nm diameter nanowire.

solid vapor surface energy, zinc addition was related to an increase in the ratio between the liquid solid and liquid vapor surface energies.

In this study, we demonstrate vertically freestanding GaAs twinning superlattice structures grown by MOVPE using zinc as an enabler (see Methods for full details). We discuss nanowire morphology for a range of diameters and report a strong correlation between diameter and superlattice period. Qualitative

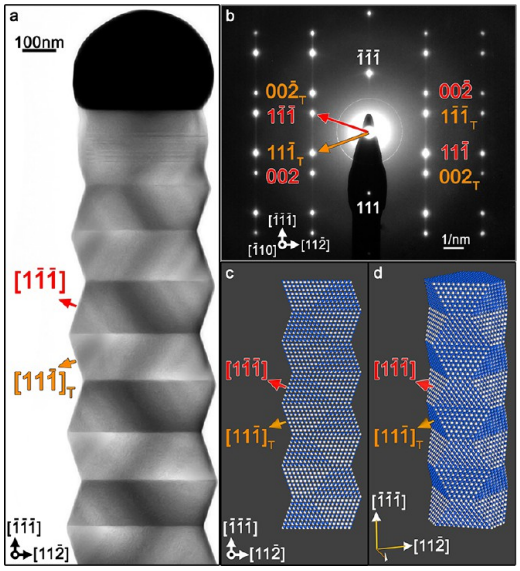

Figure 2. Exploration of the twinning superlattice structure: (a) [$\bar{1}$10] zone axis bright field TEM image with facet normals shown for two adjoining facets. The subscript T indicates that the second direction arises as a result of crystalline twinning; (b) indexed electron diffraction pattern corresponding to the image shown in (a) where the facet normals may be clearly identified as [1$\bar{1}\bar{1}$] and [11$\bar{1}$]$_T$; (c) an orthogonal projection of the same model viewed along the [$\bar{1}$10] zone axis; (d) an atomic model of the twinning superlattice structure in arbitrary perspective illustrating the alternating polarity of adjoining facets.

difference between the relationship found here and that reported previously for GaP and InP is explained with reference to expected differences in chemical potential and relevant surface energies.

RESULTS AND DISCUSSION

Figure 1 presents scanning electron microscopy (SEM) images of varying colloid treatments from the same MOVPE growth run which contrast relatively low density nanowire samples on the left (Figure 1a–c) with visibly higher density samples to the right (Figure 1b–d). The insets presented are magnified views of selected nanowire tips with those in the top row (Figure 1a,b) being approximately 50 nm in diameter and those at the bottom (Figure 1c,d), 100 nm. Of immediate note is a periodic oscillation in sidewall facet orientation with the period of oscillation increasing with increasing nanowire diameter. Importantly, this period of oscillation appears unaffected by nanowire density with the low density samples to the left (Figure 1a–c) closely resembling the higher density samples to the right (Figure 1a–c) despite a factor of approximately four difference in total length and therefore growth rate.

The origin of this periodic oscillation in sidewall faceting is explored in Figure 2. Figure 2a presents a ⟨110⟩ zone axis bright field transmission electron microscopy (TEM) image of a typical GaAs nanowire where the normals to each of the side facets observed

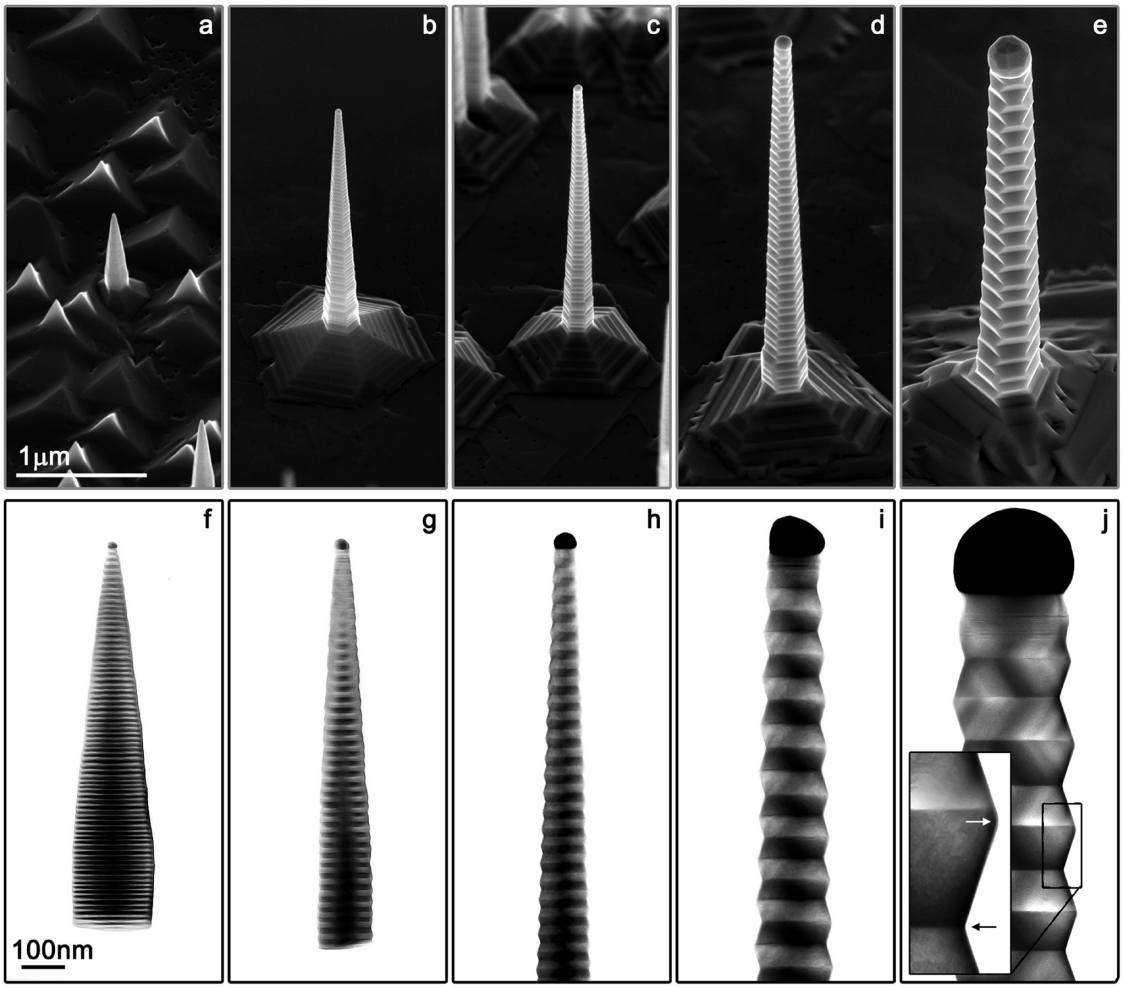

Figure 3. General morphology of the obtained GaAs twinning superlattice structures: Top row presents SEM images for each of the Au colloid diameters, (a) 10, (b) 30, (c) 50, (d) 100, and (e) 250 nm taken at a constant magnification with the sample substrate tilted 45° relative to the incident electron beam. Bottom row presents bright field TEM for each of the Au colloid diameters, (f) 10, (g) 30, (h) 50, (i) 100, and (j) 250 nm from representative nanowires taken along the ⟨110⟩ zone axis again at a constant magnification. Inset to (j) is a magnified view of the sidewall that demonstrates how the convex meeting point of facets (white arrow) appears below the twin plane with the concave meeting of facets (black arrow) appears at the twin plane.

along one sidewall profile are labeled. Indexing the corresponding zincblende selected area diffraction pattern (Figure 2b), where polarity has been inferred from the known substrate orientation,[47,48] enables these sidewall facets to be identified as belonging to the {111} family with each arising from a different crystal orientation due to rotational twinning along the ⟨111⟩ growth direction. Linking this with the clear periodicity in contrast observed along the growth direction in Figure 2a, the observed structures are thus analogous to the twinning superlattices reported previously for other III−V nanowire material systems and growth geometries.[15,19,22] An atomic model of this structure shown both in orthogonal projection along the [1$\bar{1}$0] zone axis (Figure 2c) and an arbitrary perspective (Figure 2d) additionally illustrates the alternating polarity of adjoining facets in this structure.

Being polar and nonparallel to the growth direction, {111} oriented sidewalls define a constantly varying nanowire cross section that tends toward triangular as the sidewall of one polarity type grows in area at the expense of the adjoining facets of opposite polarity. Insertion of a rotational twin reverses facet polarity at the twin plane allowing for continuation of growth to produce the well reported truncated octahedron geometry.[49,50] Where the probability of twin formation is low such that it only occurs for a given distortion of the nanowire cross section away from its equilibrium hexagonal shape, periodic twin formation may be expected along the growth direction.[15,19]

Ascending in diameter from left to right, Figure 3 presents SEM (Figure 3a−e) and TEM (Figures 3f−j) images of nanowires seeded by each of the various colloid sizes employed in this work. The distinct diameter dependence of the twin spacing is again apparent in both the sidewall faceting where visible and the contrast variation of TEM images along the growth direction. Beyond this periodic twinning the most striking feature observed is a systematic increase in nanowire length with increasing nanowire diameter.

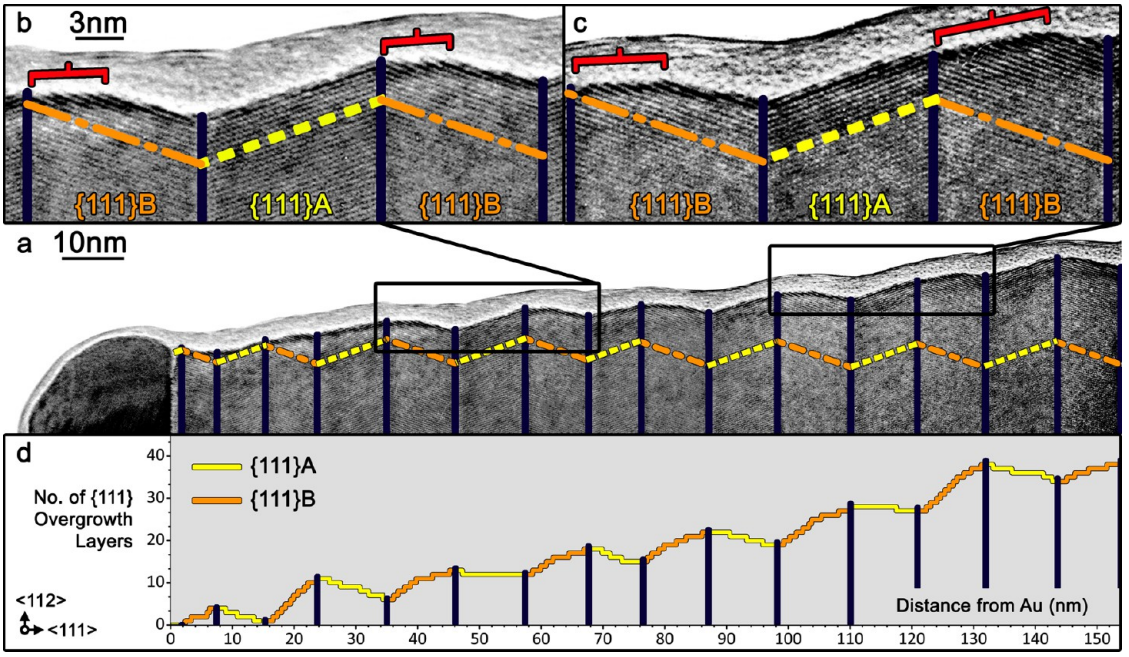

Figure 4. Investigation of sidewall growth: (a) ⟨110⟩ zone axis HRTEM image of an approximately 30 nm diameter nanowire. Twin plane locations are marked with solid dark gray lines (blue online) while dashed light gray (yellow online) and dashed dotted medium gray lines (orange online) show expected {111}A and {111}B sidewall projections, respectively; (b, c) magnified views of (a) where expected sidewall projections are again shown. Regions of the sidewall strongly deviating from the expected {111}B orientation are highlighted with dark gray square braces (red online); (d) Plot of the number of {111} bilayers difference between the expected sidewall profile and the actual sidewall.

Variation in nanowire length and therefore growth rate with areal density has already been noted in Figure 1 and is a well-established concept in the nanowire literature.[51] Authors often relate the group III diffusion length to the concept of a "collection area" around the base of the nanowires with effective competition occurring between individual nanowires when these collection areas overlap.[52,53] Where nanowire density is reduced, material supply to each individual nanowire is increased which in turn increases the growth rate to ultimately produce longer nanowires as may be observed moving between Figure 3c and d (see Figure S1 in the Supporting Information for lower magnification images). In the limit where the separation of the nanowires exceeds the effective group III diffusion length, the growth rate becomes decoupled from further reductions in density[53] and the nanowire length remains constant as is observed comparing Figure 3d and e.

Additional to the effect of density, the growth rate may also be a function of the nanowire diameter, where the Gibbs Thompson effect is significant in reducing the effective supersaturation of smaller diameter nanowires.[51,54−56] That such an effect was significant here may be appreciated by comparing the length of the smallest diameter nanowires (Figure 3a) with those of slightly larger diameter (Figure 3b). Large variation in length is furthermore noted within Figure 3a itself with pyramidal structures apparent where the Au diameter was barely above the diameter threshold for growth. We also observed pits containing spots of lighter contrast where the Au diameter was below this threshold (Figure S2 in the Supporting Information shows one such pit).

Turning now to the TEM images shown in Figure 3f−j, a region of randomly twinned zincblende is observed directly below the seed particles of both the larger diameter growths. Similar regions were observed for all nanowires excepting those of smallest diameter (Figure S3 in the Supporting Information presents TEM images acquired at a higher resolution) and have been linked in other systems to the changes in material supply with the termination of growth on cool down.[12,13] Also of note is the large increase evident in nanowire tapering with reduction in Au seed size. While radial overgrowth is expected to be a complex function of factors such as nanowire geometry and density, measurement of the difference between base and tip diameters reveals a relatively constant radial growth rate across nanowire diameters. The difference in tapering may thus be related in the first instance to the reduced axial growth rate of the smaller diameter nanowires leading to a reduced ratio of axial to radial growth.

Though radial overgrowth has mostly obscured the original {111} facets of the smaller diameter nanowires, careful examination of the larger diameter structures seen in Figure 3i,j reveals an asymmetry between the location of the twin planes and the apparent intersection of the sidewall facets. In particular, where the intersection of the sidewall facets is

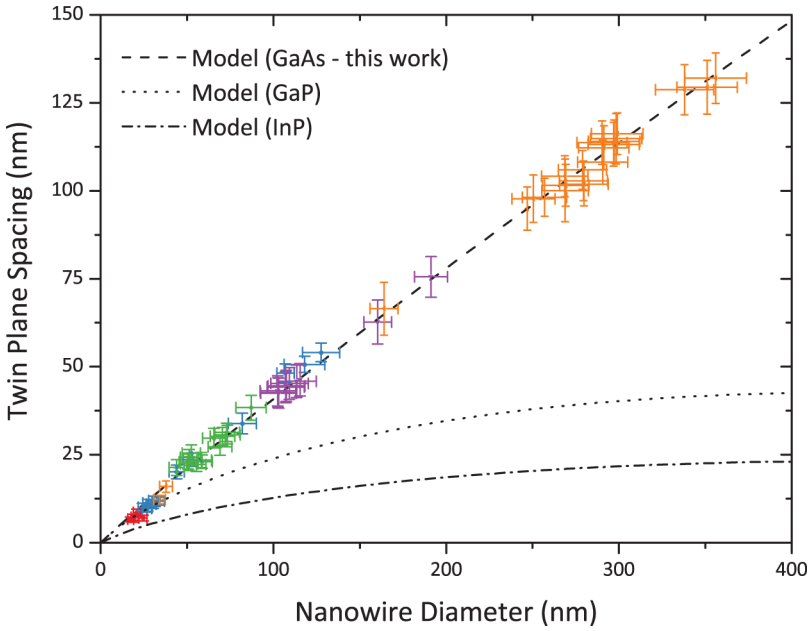

Figure 5. Plot of nanowire twinning superlattice average twin plane spacing as a function of nanowire diameter where results from each of the different colloid treatments are shown in differing colors. The error in diameter is defined as 10% for diameters of less than 150 nm and 5% for values greater than this. Variability in segment length is demonstrated by ±1 standard deviation from average. All lines are generated by eq 2, with the dashed line being a fit to the current data and the dotted and dash-dotted lines being representative fits for GaP[17] and InP[19], respectively, from previous publications.

convex it is seen to appear below the nearest twin plane, but where the intersection is concave it appears on or very close to the line of the twin plane. Similar patterns of radial overgrowth are apparent in previous reports of III−V twinning superlattice structures,[15,16,22] while asymmetry in radial overgrowth leading to the {111}A facets having a larger area than the {111}B facets has been noted for both InAs crystal phase superlattices[57] and pseudoperiodic $InAs_{(1-x)}Sb_x$ twinning superlattices.[58]

The asymmetry of radial overgrowth is investigated in Figure 4 by overlaying the expected {111} sidewall projection onto a HRTEM image of the observed sidewall. This line construction represents ideal {111} faceting and illustrates the expected sidewall position prior to radial overgrowth with the offset between it and the actual sidewall (Figure 2a) being representative of tapering due to radial overgrowth.

Taking a magnified view from close to the Au nanoparticle but outside the neck region, Figure 4b compares the actual sidewall profile of three twin segments with that expected for {111} faceting. While the sidewall profile of the middle segment closely resembles an expected {111}A orientation, those of the outer two segments show significant deviation from {111}B. Radial overgrowth appears to have transformed the sidewall profile of both these segments, with two different orientations clearly visible. Whereas the right-hand side of each segment (opposite the direction of growth) retains an orientation close to {111}B the left-hand side appears close to horizontal in the figure. Counting {111} planes it is apparent that this new sidewall orientation arises from the incomplete extension of {111} planes from the right-hand twin boundary to the left. A similar geometry is evident with further radial overgrowth, as shown in Figure 4c, though the angle formed by this incomplete extension of planes appears somewhat variable (the distribution of sidewall orientations formed by radial overgrowth on {111}B facets is presented for various nanowire diameters in Figure S4 of the Supporting Information).

Figure 4d illustrates the above observations by plotting the number of {111} planes from the expected {111} sidewall profile constructed to that of the actual sidewall observed by HRTEM. Steps in this plot represent the origin or termination of {111} bilayers with the gradient, or more specifically the deviation from horizontal, being representative of deviation from a {111} sidewall orientation. An overall increase in the number of counted planes and the related net positive gradient may furthermore be considered indicative of material added through radial overgrowth. This increase is further observed to be pseudoperiodic with a greater number of overgrowth layers at each concave intersection of facets relative to the convex intersection below. Vu *et al.*[20] have previously suggested that radial growth rate is higher at these concave intersections due to the re-entrant geometry.

Returning to Figure 4d and examining the behavior of each segment type in turn, it is first noted that the {111}A sections of the graph exhibit a low density of steps in agreement with the close to expected

orientation already discussed. These steps are furthermore universally related to the termination of {111} bilayers. Such observations contrast with the {111}B sections where a high density of steps is related to the origin of overgrowth planes. Unlike the generally uniform distribution of steps observed for the {111}A segments, there is furthermore a tendency for steps on the {111}B sections to be found more toward the left-hand side of these sections (the direction of growth). It is this grouping of steps which is responsible for the apparent change in sidewall orientation and the related asymmetry at the convex intersection of facets.

Taken together, these observations are suggestive in the first instance of an energetic instability to the {111}B as terminated facets under the current growth conditions. While contrasting with previous reports for {112} faceting,[59] detailed DFT calculations[60] suggest such an analysis would not be unreasonable given the significantly lower V/III ratio used in this work. Overgrowth morphology is, however, not only a function the various surface energies but also the total surface area generated. Interpretation is furthermore complicated by the three-dimensional nature of radial overgrowth, with recent work highlighting the potential complexity of such processes.[61,62] Finally, we note that a complete transformation of facet orientation toward {110} has been reported for InAs[21] and InP[20] twinning superlattice structures as well as regions of pseudoperiodic twinning in $InAs_{(1-x)}Sb_x$[58] nanowires.

Understanding the influence of various growth parameters on the twinning superlattice period is key to tailoring this spacing for various applications and thus realizing its full potential. Shown in Figure 5 is a plot of superlattice period as a function of nanowire tip diameter, with data from each different colloid treatment shown. Consistent results are noted for those diameters where the different treatments overlap despite differences in density and nanowire length. This confirms in a quantitative manner what was originally observed from Figure 1, that density and growth rate do not significantly affect twin spacing.

The apparent linearity of the result presented in Figure 5 is similar to that reported for ZnSe twinning superlattice nanowires,[26] but differs from the clearly nonlinear trends reported for other III−V materials, namely InAs,[15] InP,[19] and GaP.[22] Most authors have interpreted this relationship as a balance between the energy required for twin formation and the increased droplet surface energy inherent to deviation from the equilibrium cross sectional shape with the latter being geometrically similar for a given ratio of twin spacing to diameter. For sawtooth faceting in Si nanowires where twinning is absent, Ross *et al.*[63] equated a barrier to edge creation with the difference in free energy per unit length of growth for two different nonvertical sidewall facet orientations. Facet orientation was considered to change where this difference exceeded the barrier to edge creation giving a linear relationship between facet period and nanowire diameter. A similar total energy approach was also described by Shim *et al.*[64] for periodic twinning in SiC nanowires. The linear relationship between twin spacing and nanowire diameter so derived was well matched experimentally and allowed the authors to calculate a dynamic variation of less than 1° in contact angle during growth.

Taking a conceptually different route in order to describe the nonlinear relationship between diameter and twin spacing found first for InP and then GaP, Algra *et al.*[19,22] instead considered individual nucleation events. Relative nucleation probabilities were determined by finding the free energy difference between a facet conserving nucleus and its twin. For the point at which nucleation of either orientation is equally probable, a linear relationship was again derived;

$$H_c \cong \frac{b}{h}\frac{\gamma_T}{\gamma_{LV}\sin\delta_0}\left(\frac{\Gamma}{\Delta\mu}\right)\cdot D \qquad (1)$$

with H_c being the axial distance from the point where the nanowire cross section is hexagonal, $\Gamma = \gamma_{SL} + 1/6 \cdot [\gamma_{SV} - \gamma_{SV}\cos(\delta_0)]$ the effective interfacial energy barrier to nucleus formation, γ_T, γ_{SL}, γ_{SV}, and γ_{LV} the surface energies per unit area of a twin plane, the solid liquid, solid vapor, and liquid vapor interfaces, respectively, $\Delta\mu$ is the supersaturation in the Au seed, as defined by the difference in chemical potential between III−V pairs in solution relative to those in the solid, δ_0 is the angle of the droplet with respect to a {111}B facet at a hexagonal cross section (preferred nucleation sites have recently been analyzed for this geometry by Liu *et al.*[65]), h is the planar bilayer spacing in the ⟨111⟩ direction, D is the nanowire diameter, and b is a geometrical constant previously calculated to be 1.16.[22] (A schematic illustration of the geometry and parameters considered is provided in Figure S5 of the Supporting Information. The full derivation of H_c is discussed in section S6 of the Supporting Information.)

The length H_c may be considered something of a balance between an increasingly unfavorable contact angle due to the distortion of the seed particle and the energetic barrier to twin formation. As the distortion of the seed particle will be an increasing function of H_c, it is perhaps intuitive that an increased resistance to this distortion, γ_{LV}, will reduce H_c, while an increased barrier to twin formation, γ_T, will increase it. The barrier to twin formation is furthermore not only a function of γ_T, but also the interfacial area between nanowire and nucleus. As Γ will act to increase and $\Delta\mu$ reduce the critical nucleus size,[49,66] an increase in their ratio, $\Gamma/\Delta\mu$, will also act to increase the barrier to twin formation, reducing the expected value of H_c.

While H_c gives the point beyond which twin formation is energetically more favorable for an individual nucleation event, the axial distance between twin planes is ultimately the product of multiple nucleation

events. Algra *et al.*[19,22] found a good fit to their nonlinear experimental result by calculating the most probable number of uninterrupted facet conserving nucleation events ending in a twin, the total segment length H_s being less than two times the critical distance H_c;

$$H_s = 2H_c\left\{1 + \left(\frac{1}{\Delta}\right)\ln\left[1 - \exp\left(\frac{-\Delta}{H_c/h}\right)\right]\right\} \quad (2)$$

$$\Delta = \frac{c^2}{k_B T}\gamma_T\left(\frac{\Gamma}{\Delta\mu}\right)^2 \quad (3)$$

where k_B and T have their usual meanings and c is another geometrical constant previously defined as 1.98.[22] Carefully examining eq 2, it is apparent that the relationship between twinning superlattice segment length H_s and nanowire diameter D will follow the linear relationship found for H_c more closely as Δ increases. Linear behavior may thus be expected where the barrier to twin formation is high, as Δ is by definition directly proportional to this barrier for a hexagonal cross section.[19] Inspecting eq 3, this barrier is further observed to be the product of both the twin plane surface energy, γ_T, and the term $(\Gamma/\Delta\mu)^2$, which has been shown to be proportional to the interfacial area between nanowire and nucleus, where the nanowire cross section is hexagonal.[49] (The variation of H_s as a function of several physical parameters is graphed in Figure S6 of the Supporting Information. The behavior so observed gives an indication of how the relationship between twin spacing and nanowire diameter may be expected to change with varying growth conditions.)

With a significant barrier to twin formation, Δ, the probability of a twin or facet changing nucleation event is reduced and the likelihood of an uninterrupted sequence of facet conserving nuclei approaching the length H_s predicted through energetics is increased. In the case of GaAs, the twin plane formation energy has been reported[67] as 2.75×10^{-2} J/m^2, which is higher than the corresponding values of 2.10×10^{-2} J/m^2 and 9.00×10^{-3} J/m^2 reported for GaP[67] and InP,[67] respectively. Turning to Γ, the dominating contribution to this term is γ_{SL}, which for Au on planar GaAs can be approximated by γ_{SV}.[19,66] For GaAs, γ_{SV} of a {111}B surface under relatively low V/III ratios has been calculated[60] to be 1.11 J/m^2, which is again higher than the values of 0.96 and 0.8 J/m^2 reported for GaP[22] and InP,[19,68] respectively. With higher surface energies related to both twin plane formation and the generation of solid−liquid interface, it may be thus expected that, as observed experimentally, the relationship between twin spacing and nanowire diameter will better approximate the linear behavior found for H_s in GaAs relative to both GaP and InP.

Returning to Figure 5, a fit of eq 2 to the data in this work is shown where the above values for GaAs have been used in conjunction with the value of γ_{LV} calculated by Algra *et al.*[22] for a trimethylgallium partial pressure most closely matching our own. The values of the remaining parameters that give the best fit are $\delta_0 = 17°$ and $\Delta\mu = 191$ meV per pair. The first of these values is only 10° larger than the value extracted for GaP by similar means,[22] while the second fit parameter, supersaturation, is significantly lower than that found for GaP in the same work.[22] The latter trend corresponds well with the work of Glas[69] who has previously employed chemical thermodynamics to calculate the supersaturation relevant to Au seeded GaP nanowire growth as being higher than that for Au seeded GaAs nanowire growth at the same temperature and seed particle composition (Au, Ga, group V element). Where growth temperature was raised, as is the case for this work relative to the previous reports of twinning superlattice formation in both GaP and InP, the calculated supersaturation was furthermore also found to be lowered. Taking the value of supersaturation found here by fitting, the calculations of Glas[69] suggest that the Ga content of the Au alloy was between 40 and 60% during growth, a range similar to that reported and calculated in other work.[70−73]

In making the above fit, we have implicitly assumed a constant supersaturation $\Delta\mu$ across all samples. This is perhaps counterintuitive given the differences in growth rate observed from Figure 1. Nucleation probability is however well-known to be an exponential function of liquid phase supersaturation[74−76] (see section S8 of the Supporting Information for the form of this relationship). Where the growth of each bilayer proceeds from a single nucleation event and supersaturation is approximated to be constant, the overall nanowire growth rate becomes proportional to this nucleation rate.[74] In such a regime, only a small change in supersaturation is required to generate the observed change in growth rate, thus rendering any related change in superlattice period likely within the error bounds of this work. Alternatively, where supersaturation is considered to periodically fluctuate, as emphasized by small nanowire diameters or low reactant solubility, the strong exponential dependence of nucleation probability effectively defines a constant supersaturation for which nucleation is expected.[75,76] We further note that $\Delta\mu$ has previously been calculated to be only a weak function of gallium supply rate and thus growth rate for GaP twinning superlattice growth under similar reactor conditions.[22] Such a scenario explains our initial observation that the twinning superlattice period is unaffected by density and related growth rate.

Returning to the given equations, it has been noted that $\Delta\mu$ acts to reduce the critical nucleus size and thus appears in the denominator of both eqs 1 and 3. As such, it may be appreciated that the decreased supersaturation value of GaAs in comparison to GaP works to increase both twin spacing and the linearity of the

spacing *versus* diameter relationship. This qualitative difference in behavior is illustrated in Figure 5 where previous fits of eq 2 to both GaP[22] and InP[19] twinning superlattice structures are shown for comparison. The higher twin plane, surface and interfacial energies relevant to GaAs nanowire growth coupled with relatively low chemical potential all act to generate a significant difference in superlattice period at larger diameter. Although the relationship between diameter and twin spacing found for GaAs is almost exactly linear, we note that the model presented here (eqs 1−3) provides an even better fit to the experimental data (see Supporting Information, section S9) in addition to describing the differences in behavior between material systems.

CONCLUSIONS

In conclusion, we have demonstrated twinning superlattice formation in vertically standing GaAs nanowires. Studying nanowire morphology across a range of diameters and densities, we have shown that under the current growth conditions, twin plane spacing and, by implication, supersaturation are not strong functions of nanowire areal density. A polarity dependence to radial overgrowth has also been noted with the orientation of expected {111}B facets being seen to be altered in a specific fashion. Whereas previous studies of periodic twinning in InP[19] and GaP[22] found a nonlinear relationship between twin spacing and nanowire diameter, we find an approximately linear relationship. Taking the model used to fit these previous nonlinear results, we have shown how the higher twin plane and surface energies of GaAs coupled with lower chemical potential may act to generate this behavior. Beyond growth parameter tuning, the model also provides an indirect measure of some fundamental physical parameters affecting nanowire growth and a method to assess the effect of various growth conditions, such as doping, on these parameters. The availability of such a model provides a useful tool for the future investigation of the novel electronic, thermal, and mechanical properties predicted to arise from periodic twinning.

METHODS

Nanowires were grown *via* horizontal flow metalorganic vapor phase epitaxy (MOVPE) utilizing an Aixtron 200/4 reactor operating at a pressure of 100 mbar and a flow of 15 standard L/min.[77] A growth temperature of 575 °C was used in conjunction with AsH_3 and trimethylgallium (TMG) molar fractions of 1.43×10^{-5} and 1.04×10^{-5}, respectively, to give a V/III ratio of approximately 1.4. Growth time was 60 min, including a 2 min nucleation window before the introduction of diethylzinc (DEZn) at a molar fraction of 1.4×10^{-4} to generate the TSL structure. Following termination of TMG and DEZn flows, AsH_3 flow was maintained until the reactor reached a temperature of 350 °C. Growth was conducted on semi-insulating GaAs(111)B substrates which had been individually treated with various concentrations of 10, 30, 50, 100, and 250 nm colloidal Au solutions (Ted Pella, Inc.). Subsequent investigation by both scanning electron microscopy (SEM) and transmission electron microscopy (TEM) was performed utilizing a FEI Helios 600 NanoLab Dualbeam (FIB/SEM) operated at 10 kV and a Phillips CM300 TEM operated at 300 kV, respectively. Samples for TEM investigation were prepared by mechanical dispersion on holey carbon copper grids.

Most data points in Figure 5 were obtained from SEM images where the error for diameter measurement has been conservatively estimated at ±10% for diameters less than 150 nm and ±5% for diameters greater than this. Systematic error is expected in SEM calibration but assuming good astigmatism correction, error should cancel in the ratio of superlattice period to diameter. As may be expected there was some dispersion in superlattice period (Figure S7 of the Supporting Information, section S10, presents the measured distributions for various diameter nanowires) and the error bars shown equate to one standard deviation from average.

Conflict of Interest: The authors declare no competing financial interest.

Supporting Information Available: Lower magnification SEM showing nanowire areal density, high magnification SEM demonstrating the Gibbs Thompson effect, lattice resolved high resolution TEM, distribution of sidewall orientations as altered from the expected{111}B orientation by overgrowth, schematic illustration of the geometry and physical parameters used in modeling, discussion, and derivation of H_c used in this work, numerical illustration of the modeled segment length behavior, definition and discussion of the relationship between supersaturation and growth rate, comparison of a linear fit with that of the presented model, and distribution of twin plane spacing. This material is available free of charge *via* the Internet at http://pubs.acs.org.

Acknowledgment. This research is supported by the Australian Research Council. Authors thank the Australian National Fabrication Facility for access to the growth and microscopy facilities and Centre for Advanced Microscopy and Australian Microscopy and Microanalysis Research Facility for access to microscopy facilities used in this work.

REFERENCES AND NOTES

1. Wallentin, J.; Anttu, N.; Asoli, D.; Huffman, M.; Åberg, I.; Magnusson, M. H.; Siefer, G.; Fuss-Kailuweit, P.; Dimroth, F.; Witzigmann, B.; *et al.* InP Nanowire Array Solar Cells Achieving 13.8% Efficiency by Exceeding the Ray Optics Limit. *Science* **2013**, *339*, 1057–1060.
2. Holm, J. V.; Jørgensen, H. I.; Krogstrup, P.; Nygård, J.; Liu, H.; Aagesen, M. Surface-Passivated GaAsP Single-Nanowire Solar Cells Exceeding 10% Efficiency Grown on Silicon. *Nat. Commun.* **2013**, *4*, 1498.
3. Heurlin, M.; Wickert, P.; Falt, S.; Borgström, M. T.; Deppert, K.; Samuelson, L.; Magnusson, M. H. Axial InP Nanowire Tandem Junction Grown on a Silicon Substrate. *Nano Lett.* **2011**, *11*, 2028–2031.
4. Krogstrup, P.; Jorgensen, H. I.; Heiss, M.; Demichel, O.; Holm, J. V.; Aagesen, M.; Nygard, J.; Fontcuberta i Morral, A. Single-Nanowire Solar Cells Beyond the Shockley-Queisser Limit. *Nat. Photonics* **2013**, *7*, 306–310.
5. Svensson, J.; Anttu, N.; Vainorius, N.; Borg, B. M.; Wernersson, L.-E. Diameter-Dependent Photocurrent in InAsSb Nanowire Infrared Photodetectors. *Nano Lett.* **2013**, *13*, 1380–1385.
6. Pettersson, H.; Tragardh, J.; Persson, A. I.; Landin, L.; Hessman, D.; Samuelson, L. Infrared Photodetectors in Heterostructure Nanowires. *Nano Lett.* **2006**, *6*, 229–232.
7. Hua, B.; Motohisa, J.; Kobayashi, Y.; Hara, S.; Fukui, T. Single GaAs/GaAsP Coaxial Core-Shell Nanowire Lasers. *Nano Lett.* **2009**, *9*, 112–116.

8. Ganjipour, B.; Dey, A. W.; Borg, B. M.; Ek, M.; Pistol, M.-E.; Dick, K. A.; Wernersson, L.-E.; Thelander, C. High Current Density Esaki Tunnel Diodes Based on GaSb-InAsSb Heterostructure Nanowires. *Nano Lett.* **2011**, *11*, 4222–4226.
9. Wallentin, J.; Persson, J. M.; Wagner, J. B.; Samuelson, L.; Deppert, K.; Borgstrom, M. T. High-Performance Single Nanowire Tunnel Diodes. *Nano Lett.* **2010**, *10*, 974–979.
10. Tomioka, K.; Yoshimura, M.; Fukui, T. A III-V Nanowire Channel on Silicon for High-Performance Vertical Transistors. *Nature* **2012**, *488*, 189–192.
11. Egard, M.; Johansson, S.; Johansson, A. C.; Persson, K. M.; Dey, A. W.; Borg, B. M.; Thelander, C.; Wernersson, L. E.; Lind, E. Vertical InAs Nanowire Wrap Gate Transistors with $f_t > 7$ GHz and $f_{max} > 20$ GHz. *Nano Lett.* **2010**, *10*, 809–812.
12. Joyce, H. J.; Wong-Leung, J.; Gao, Q.; Tan, H. H.; Jagadish, C. Phase Perfection in Zinc Blende and Wurtzite III-V Nanowires Using Basic Growth Parameters. *Nano Lett.* **2010**, *10*, 908–915.
13. Dick, K. A.; Caroff, P.; Bolinsson, J.; Messing, M. E.; Johansson, J.; Deppert, K.; Wallenberg, L. R.; Samuelson, L. Control of III-V Nanowire Crystal Structure by Growth Parameter Tuning. *Semicond. Sci. Technol.* **2010**, *25*, 24009.
14. Givargizov, E. I. Oriented Growth of Whiskers of $A^{III}B^{V}$ Compounds by VLS-Mechanism. *Krist. Tech.* **1975**, *10*, 473–484.
15. Caroff, P.; Dick, K. A.; Johansson, J.; Messing, M. E.; Deppert, K.; Samuelson, L. Controlled Polytypic and Twin-Plane Superlattices in III-V Nanowires. *Nat. Nanotechnol.* **2009**, *4*, 50–55.
16. Johansson, J.; Dick, K. A.; Caroff, P.; Messing, M. E.; Bolinsson, J.; Deppert, K.; Samuelson, L. Diameter Dependence of the Wurtzite-Zinc Blende Transition in InAs Nanowires. *J. Phys. Chem. C* **2010**, *114*, 3837–3842.
17. Kim, H. S.; Myung, Y.; Cho, Y. J.; Jang, D. M.; Jung, C. S.; Park, J.; Ahn, J.-P. Three-Dimensional Structure of Twinned and Zigzagged One-Dimensional Nanostructures Using Electron Tomography. *Nano Lett.* **2010**, *10*, 1682–1691.
18. Grap, T.; Rieger, T.; Ch, B.; Th, S.; Grützmacher, D.; Lepsa, M. I. Self-Catalyzed VLS Grown InAs Nanowires with Twinning Superlattices. *Nanotechnology* **2013**, *24*, 335601.
19. Algra, R. E.; Verheijen, M. A.; Borgstrom, M. T.; Feiner, L. F.; Immink, G.; van Enckevort, W. J. P.; Vlieg, E.; Bakkers, E. Twinning Superlattices in Indium Phosphide Nanowires. *Nature* **2008**, *456*, 369–372.
20. Vu, T. T. T.; Tilman, Z.; Verheijen, M. A.; Plissard, S. R.; Immink, G. W. G.; Haverkort, J. E. M.; Bakkers, E. P. A. M. High Optical Quality Single Crystal Phase Wurtzite and Zincblende InP Nanowires. *Nanotechnology* **2013**, *24*, 115705.
21. Ghalamestani, S. G.; Heurlin, M.; Wernersson, L.-E.; Lehmann, S.; Dick, K. A. Growth of InAs/InP Core−Shell Nanowires with Various Pure Crystal Structures. *Nanotechnology* **2012**, *23*, 285601.
22. Algra, R. E.; Verheijen, M. A.; Feiner, L.-F.; Immink, G. G. W.; Enckevort, W. J. P. v.; Vlieg, E.; Bakkers, E. P. A. M. The Role of Surface Energies and Chemical Potential During Nanowire Growth. *Nano Lett.* **2011**, *11*, 1259–1264.
23. Dowdy, R.; Mohseni, P.; Fortuna, S. A.; Jianguo, W.; Xiuling, L. Twinning Superlattice in VLS Grown Planar GaAs Nanowires Induced by Impurity Doping.Photonics Conference (IPC), 2012 IEEE, Burlingame, CA Sept. 23−27, 2012, **2012**; IEEE: New York, **2012**; pp 693−694.
24. Shen, G.; Chen, P. C.; Bando, Y.; Golberg, D.; Zhou, C. Single-Crystalline and Twinned Zn_3P_2 Nanowires: Synthesis, Characterization, and Electronic Properties. *J. Phys. Chem. C* **2008**, *112*, 16405–16410.
25. Meng, Q.; Jiang, C.; Mao, S. X. Temperature-Dependent Growth of Zinc-Blende-Structured ZnTe Nanostructures. *J. Cryst. Growth* **2008**, *310*, 4481–4486.
26. Li, Q.; Gong, X.; Wang, C.; Wang, J.; Ip, K.; Hark, S. Size-Dependent Periodically Twinned ZnSe Nanowires. *Adv. Mater.* **2004**, *16*, 1436–1440.
27. Fan, X.; Meng, X. M.; Zhang, X. H.; Zhang, M. L.; Jie, J. S.; Zhang, W. J.; Lee, C. S.; Lee, S. T. Formation and Photoelectric Properties of Periodically Twinned ZnSe/SiO_2 Nanocables. *J. Phys. Chem. C* **2009**, *113*, 834–838.
28. Wang, Y. Q.; Philipose, U.; Xu, T.; Ruda, H. E.; Kavanagh, K. L. Twinning Modulation in ZnSe Nanowires. *Semicond. Sci. Technol.* **2007**, *22*, 175.
29. Hao, Y. F.; Meng, G. W.; Wang, Z. L.; Ye, C. H.; Zhang, L. D. Periodically Twinned Nanowires and Polytypic Nanobelts of ZnS: The Role of Mass Diffusion in Vapor-Liquid-Solid Growth. *Nano Lett.* **2006**, *6*, 1650–1655.
30. Wang, J.; Sun, X. W.; Xie, S.; Zhou, W.; Yang, Y. Single-Crystal and Twinned Zn_2SnO_4 Nanowires with Axial Periodical Structures. *Cryst. Growth Des.* **2007**, *8*, 707–710.
31. Kim, S.; Na, S.; Jeon, H.; Lee, B.; Yang, J.; Kim, H.; Lee, H. J. Effects of Sn Doping on the Growth Morphology and Electrical Properties of ZnO Nanowires. *Nanotechnology* **2013**, *24*, 065703.
32. Wang, D.-H.; Di, X.; Qing, W.; Ya-Juan, H.; Guo-Qiang, J.; Xiang-Yun, G.; Tu, K. N. Periodically Twinned SiC Nanowires. *Nanotechnology* **2008**, *19*, 215602.
33. Ikonić, Z.; Srivastava, G. P.; Inkson, J. C. Electronic Properties of Twin Boundaries and Twinning Superlattices in Diamond-Type and Zinc-Blende-Type Semiconductors. *Phys. Rev. B* **1993**, *48*, 17181–17193.
34. Ikonić, Z.; Srivastava, G. P.; Inkson, J. C. Optical Properties of Twinning Superlattices in Diamond-Type and Zinc-Blende-Type Semiconductors. *Phys. Rev. B* **1995**, *52*, 14078–14085.
35. Tadic, M.; Ikonić, Z. The Multiband Effective-Mass Model of the Electronic Structure and Intersubband Absorption in p-Type-Doped Twinning Superlattices. *J. Phys.: Condens. Matter* **1999**, *11*, 6891.
36. Tsuzuki, H.; Cesar, D. F.; Rebello de Sousa Dias, M.; Castelano, L. K.; Lopez-Richard, V.; Rino, J. P.; Marques, G. E. Tailoring Electronic Transparency of Twin-Plane 1D Superlattices. *ACS Nano* **2011**, *5*, 5519–5525.
37. Akiyama, T.; Yamashita, T.; Nakamura, K.; Ito, T. Band Alignment Tuning in Twin-Plane Superlattices of Semiconductor Nanowires. *Nano Lett.* **2010**, *10*, 4614–4618.
38. Shimamura, K.; Yuan, Z.; Shimojo, F.; Nakano, A. Effects of Twins on the Electronic Properties of GaAs. *Appl. Phys. Lett.* **2013**, *103*, 022105–4.
39. Moore, A. L.; Saha, S. K.; Prasher, R. S.; Shi, L. Phonon Backscattering and Thermal Conductivity Suppression in Sawtooth Nanowires. *Appl. Phys. Lett.* **2008**, *93*, 083112.
40. Sansoz, F. Surface Faceting Dependence of Thermal Transport in Silicon Nanowires. *Nano Lett.* **2011**, *11*, 5378–82.
41. Nika, D. L.; Cocemasov, A. I.; Isacova, C. I.; Balandin, A. A.; Fomin, V. M.; Schmidt, O. G. Suppression of Phonon Heat Conduction in Cross-Section-Modulated Nanowires. *Phys. Rev. B* **2012**, *85*.
42. Weathers, A.; Moore, A. L.; Pettes, M. T.; Salta, D.; Kim, J.; Dick, K.; Samuelson, L.; Linke, H.; Caroff, P.; Shi, L. Phonon Transport and Thermoelectricity in Defect-Engineered InAs Nanowires. *MRS Proc.* **2012**, 1404.
43. Deng, C.; Sansoz, F. Near-Ideal Strength in Gold Nanowires Achieved through Microstructural Design. *ACS Nano* **2009**, *3*, 3001–3008.
44. Wang, J.; Sansoz, F.; Huang, J.; Liu, Y.; Sun, S.; Zhang, Z.; Mao, S. X. Near-Ideal Theoretical Strength in Gold Nanowires Containing Angstrom Scale Twins. *Nat. Commun.* **2013**, *4*, 1742.
45. Borgstrom, M. T.; Norberg, E.; Wickert, P.; Nilsson, H. A.; Tragardh, J.; Dick, K. A.; Statkute, G.; Ramvall, P.; Deppert, K.; Samuelson, L. Precursor Evaluation for *In Situ* InP Nanowire Doping. *Nanotechnology* **2008**, *19*, 445602.
46. Wallentin, J.; Ek, M.; Wallenberg, L. R.; Samuelson, L.; Deppert, K.; Borgström, M. T. Changes in Contact Angle of Seed Particle Correlated with Increased Zincblende Formation in Doped InP Nanowires. *Nano Lett.* **2010**, *10*, 4807–4812.
47. Ek, M.; Borgström, M. T.; Karlsson, L. S.; Hetherington, C. J. D.; Wallenberg, L. R. Electron Image Series Reconstruction of Twin Interfaces in InP Superlattice Nanowires. *Microsc. Microanal.* **2011**, *17*, 752–758.

48. de la Mata, M.; Magen, C.; Gazquez, J.; Utama, M. I. B.; Heiss, M.; Lopatin, S.; Furtmayr, F.; Fernández-Rojas, C. J.; Peng, B.; Morante, J. R.; *et al.* Polarity Assignment in ZnTe, GaAs, ZnO, and GaN-AlN Nanowires from Direct Dumbbell Analysis. *Nano Lett.* **2012**, *12*, 2579–2586.
49. Johansson, J.; Karlsson, L. S.; Svensson, C. P. T.; Martensson, T.; Wacaser, B. A.; Deppert, K.; Samuelson, L.; Seifert, W. Structural Properties of (111)B-Oriented III–V Nanowires. *Nat. Mater.* **2006**, *5*, 574–580.
50. Karlsson, L. S.; Dick, K. A.; Wagner, J. B.; Malm, J. O.; Deppert, K.; Samuelson, L.; Wallenberg, L. R. Understanding the 3D Structure of GaAs ⟨111⟩B Nanowires. *Nanotechnology* **2007**, *18*, 85717.
51. Dubrovskii, V. G.; Sibirev, N. V.; Cirlin, G. E.; Soshnikov, I. P.; Chen, W. H.; Larde, R.; Cadel, E.; Pareige, P.; Xu, T.; Grandidier, B.; *et al.* Gibbs-Thomson and Diffusion-Induced Contributions to the Growth Rate of Si, InP, and GaAs Nanowires. *Phys. Rev. B* **2009**, *79*, 205316.
52. Jensen, L. E.; Bjork, M. T.; Jeppesen, S.; Persson, A. I.; Ohlsson, B. J.; Samuelson, L. Role of Surface Diffusion in Chemical Beam Epitaxy of InAs Nanowires. *Nano Lett.* **2004**, *4*, 1961–1964.
53. Persson, A. I.; Froberg, L. E.; Jeppesen, S.; Bjork, M. T.; Samuelson, L. Surface Diffusion Effects on Growth of Nanowires by Chemical Beam Epitaxy. *J. Appl. Phys.* **2007**, *101*, 34313.
54. Caroff, P.; Messing, M. E.; Borg, B. M.; Dick, K. A.; Deppert, K.; Wernersson, L. E. InSb Heterostructure Nanowires: MOVPE Growth under Extreme Lattice Mismatch. *Nanotechnology* **2009**, *20*, 95606.
55. Givargizov, E. I. Fundamental Aspects of VLS Growth. *J. Cryst. Growth* **1975**, *31*, 20–30.
56. Dubrovskii, V. G. Refinement of the Wagner-Ellis Formula for the Minimum Radius and the Givargizov-Chernov Formula for the Growth Rate of Nanowire. *Technol. Phys. Lett.* **2013**, *39*, 157–160.
57. Bolinsson, J.; Caroff, P.; Mandl, B.; Dick, K. A. Wurtzite–Zincblende Superlattices in InAs Nanowires Using a Supply Interruption Method. *Nanotechnology* **2011**, *22*, 265606.
58. Xu, T.; Dick, K. A.; Plissard, S.; Nguyen, T. H.; Makoudi, Y.; Berthe, M.; Nys, J.-P.; Wallart, X.; Grandidier, B.; Caroff, P. Faceting, Composition and Crystal Phase Evolution in III–V Antimonide Nanowire Heterostructures Revealed by Combining Microscopy Techniques. *Nanotechnology* **2012**, *23*, 095702.
59. Zou, J.; Paladugu, M.; Wang, H.; Auchterlonie, G. J.; Guo, Y. N.; Kim, Y.; Gao, Q.; Joyce, H. J.; Tan, H. H.; Jagadish, C. Growth Mechanism of Truncated Triangular III–V Nanowires. *Small* **2007**, *3*, 389–393.
60. Moll, N.; Kley, A.; Pehlke, E.; Scheffler, M. GaAs Equilibrium Crystal Shape from First Principles. *Phys. Rev. B* **1996**, *54*, 8844–8855.
61. Heiss, M.; Fontana, Y.; Gustafsson, A.; Wüst, G.; Magen, C.; O'Regan, D. D.; Luo, J. W.; Ketterer, B.; Conesa-Boj, S.; Kuhlmann, A. V.; *et al.* Self-Assembled Quantum Dots in a Nanowire System for Quantum Photonics. *Nat. Mater.* **2013**, *12*, 439–444.
62. Zheng, C.; Wong-Leung, J.; Gao, Q.; Tan, H. H.; Jagadish, C.; Etheridge, J. Polarity-Driven 3-Fold Symmetry of GaAs/AlGaAs Core Multishell Nanowires. *Nano Lett.* **2013**, *13*, 3742–3748.
63. Ross, F. M.; Tersoff, J.; Reuter, M. C. Sawtooth Faceting in Silicon Nanowires. *Phys. Rev. Lett.* **2005**, *9514*, 6104.
64. Shim, H. W.; Zhang, Y.; Huang, H. Twin Formation During SiC Nanowire Synthesis. *J. Appl. Phys.* **2008**, *104*, 063511.
65. Xiaolong, L.; Dubrovskii, V. G.; Xiaomin, R. The Nucleation Site Selection of Vapour–Liquid–Solid Nanowires. *J. Phys.: Condens. Matter* **2013**, *25*, 215302.
66. Glas, F.; Harmand, J. C.; Patriarche, G. Why Does Wurtzite Form in Nanowires of III–V Zinc Blende Semiconductors? *Phys. Rev. Lett.* **2007**, *99*, 6101.
67. Gottschalk, H.; Patzer, G.; Alexander, H. Stacking Fault Energy and Ionicity of Cubic III-V Compounds. *Phys. Status Solidi A* **1978**, *45*, 207–217.
68. Liu, Q. K. K.; Moll, N.; Scheffler, M.; Pehlke, E. Equilibrium Shapes and Energies of Coherent Strained InP Islands. *Phys. Rev. B* **1999**, *60*, 17008–17015.
69. Glas, F. Chemical Potentials for Au-Assisted Vapor-Liquid-Solid Growth of III–V Nanowires. *J. Appl. Phys.* **2010**, *108*, 073506.
70. Harmand, J. C.; Patriarche, G.; Pere-Laperne, N.; Merat-Combes, M. N.; Travers, L.; Glas, F. Analysis of Vapor–Liquid–Solid Mechanism in Au-Assisted GaAs Nanowire Growth. *Appl. Phys. Lett.* **2005**, *87*, 3101.
71. Soda, M.; Rudolph, A.; Schuh, D.; Zweck, J.; Bougeard, D.; Reiger, E. Transition from Au to Pseudo-Ga Catalyzed Growth Mode Observed in GaAs Nanowires Grown by Molecular Beam Epitaxy. *Phys. Rev. B* **2012**, *85*, 245450.
72. Piccin, M.; Bais, G.; Grillo, V.; Jabeen, F.; De Franceschi, S.; Carlino, E.; Lazzarino, M.; Romanato, F.; Businaro, L.; Rubini, S.; *et al.* Growth by Molecular Beam Epitaxy and Electrical Characterization of GaAs Nanowires. *Phys. E* **2007**, *37*, 134–137.
73. Chatillon, C.; Hodaj, F.; Pisch, A. Thermodynamics of GaAs Nanowire MBE Growth with Gold Droplets. *J. Cryst. Growth* **2009**, *311*, 3598–3608.
74. Dubrovskii, V. G.; Sibirev, N. V. General Form of the Dependences of Nanowire Growth Rate on the Nanowire Radius. *J. Cryst. Growth* **2007**, *304*, 504–513.
75. Wen, C. Y.; Tersoff, J.; Reuter, M. C.; Stach, E. A.; Ross, F. M. Step-Flow Kinetics in Nanowire Growth. *Phys. Rev. Lett.* **2010**, *105*, 195502.
76. Dubrovskii, V. G. Self-Regulated Pulsed Nucleation in Catalyzed Nanowire Growth. *Phys. Rev. B* **2013**, *87*, 195426.
77. Joyce, H. J.; Gao, Q.; Tan, H. H.; Jagadish, C.; Kim, Y.; Fickenscher, M. A.; Perera, S.; Hoang, T. B.; Smith, L. M.; Jackson, H. E.; *et al.* High Purity GaAs Nanowires Free of Planar Defects: Growth and Characterization. *Adv. Funct. Mater.* **2008**, *18*, 3794–3800.